ACS APPLIED ENERGY MATERIALS

www.acsaem.org Letter

Regulating the Solvation Structure of Potassium Ions Using a Multidentate Ether in Potassium Metal Batteries

Chao Chen, Ji Zhou, Wenbin Gong, Xueying Fan, Xiaodong Meng, Shang Chen, Longhua Sun, Yongqiang Meng, Kangjia Tao, Burak Ülgüt, Pingchuan Sun, Christopher W. Bielawski, and Jianxin Geng*

Cite This: *ACS Appl. Energy Mater.* 2022, 5, 10366−10374 Read Online

ACCESS | Metrics & More | Article Recommendations | Supporting Information

ABSTRACT: Potassium (K) is regarded as an alternative to lithium (Li) for use in contemporary energy storage devices owing to its high abundance and low electrochemical potential. However, because K ions are larger than Li ions, they exhibit different solvation properties that can ultimately affect device performance. Herein, a multidentate ether-based electrolyte is demonstrated to effectively solvate K ions and the solvation structures can be further modulated with cosolvents. The use of the multidentate ether-based electrolyte also suppresses the formation of K dendrites and significantly enhances the cycling stability of K//K symmetric cells (e.g., over 2000 h at 0.25 mA cm^{-2}).

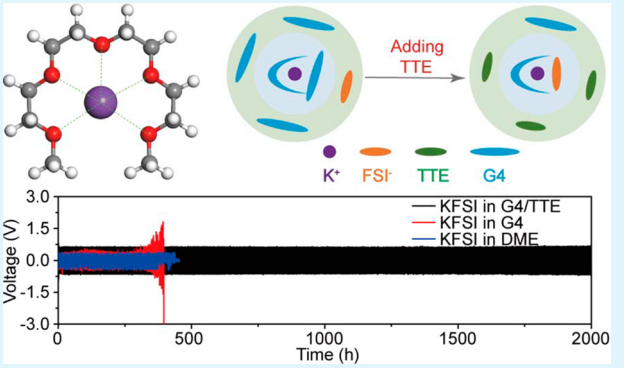

KEYWORDS: *ether-based electrolytes, multidentate solvents, solvation structures, potassium metal anode, dendrite-free metal anode*

To address the ongoing energy shortage and environmental challenges that pertain to the use of fossil fuels, the development of high-performance energy storage technologies has become a research topic of high contemporary importance.[1−4] Lithium ion batteries (LIBs) are widely used in portable electronic devices and electric vehicles. Unfortunately, the low natural abundance of lithium (only 0.0017 wt % in the earth's crust) has raised concerns about the future demands of LIBs. For comparison, sodium and potassium are markedly more abundant (2.36 and 2.09 wt %, respectively) than lithium. Potassium also has a relatively low electrochemical potential (E_{K/K^+} = −2.93 V vs the standard hydrogen electrode), which bestows potassium ion batteries (PIBs) with a wider operation voltage window and thus a higher energy density. When used as an anode metal, potassium suffers from a number of fundamental issues, particularly the formation of dendrites and an irreversible consumption of the metal due to the repeated formation of solid−electrolyte interface (SEI) layers.[5] To achieve uniform potassium stripping and plating, significant efforts have been directed toward anode development, including the use of alloys,[6] the creation of artificial SEI layers,[7] the use of three-dimensional (3D) frameworks as potassium hosts,[8] the use of 3D anode current collectors,[9] and the electrochemical polishing of potassium metal.[10] However, the overall development of PIBs lags behind that of the LIBs.

A major difference between PIBs and LIBs is the size of the constituent cations: the radius of K^+ (0.138 nm) is nearly twice as that of Li^+ (0.076 nm). Therefore, due to differences in charge distribution,[11] potassium ions are typically less solvated than their lithium ions counterparts, which thus explains why PIBs show relatively poor performance when compared to LIBs, especially in terms of cycling stability. In lithium metal batteries, carbonate-based solvents are predominately used; however, they are not suitable for potassium metal batteries due to the side reactions that occur between the solvents and potassium metal.[12] The solvated cation structure is also influenced by the electrolyte, which is a key component that facilitates ion transport and mediates the surface properties of the metal anodes found in metal batteries. A variety of electrolytes, including those that are ether-based[13] and highly concentrated,[14] room-temperature ionic liquid electrolytes,[15] and polymer-gel electrolytes,[16] have been explored to improve the performance of potassium metal batteries. However, these electrolytes suffer from low ionic conductivity, high viscosity, and/or high cost, and the solvation structures of the attendant K ions remain largely unexplored.

Received: May 16, 2022
Accepted: August 15, 2022
Published: August 19, 2022

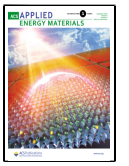

https://doi.org/10.1021/acsaem.2c01504
ACS Appl. Energy Mater. 2022, 5, 10366−10374

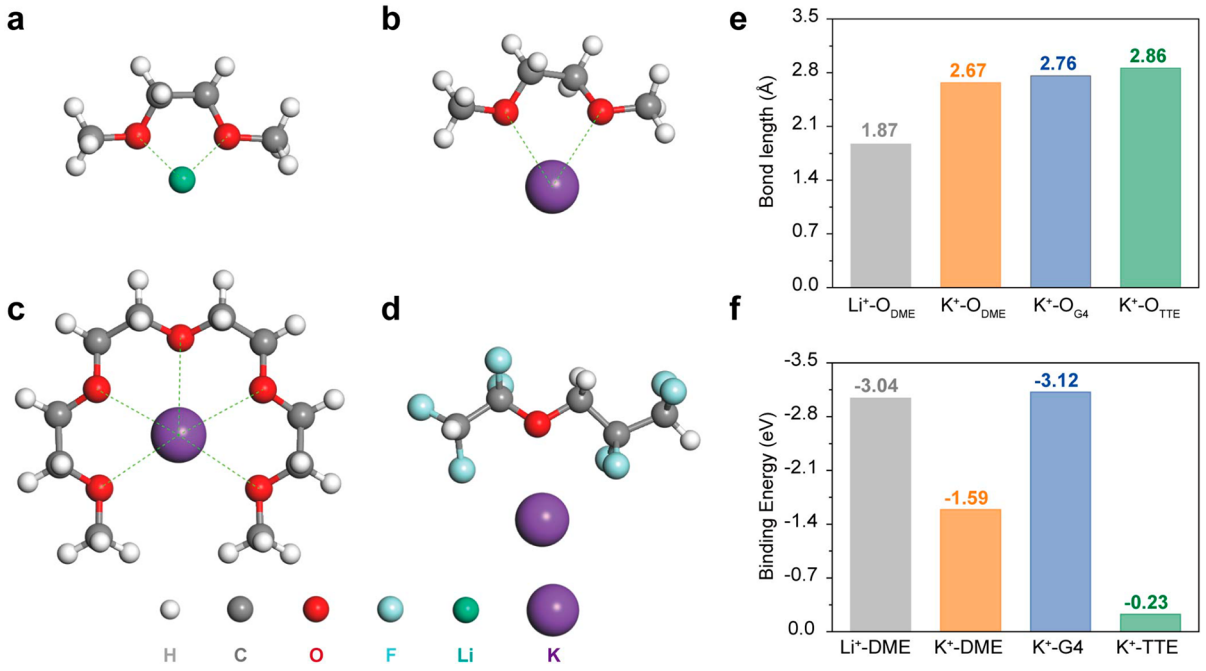

Figure 1. DFT calculations of the interactions formed between different solvents and Li^+ or K^+. (a–d) Molecular models of different solvation structures: (a) DME complexed with Li^+, (b) DME complexed with K^+, (c) G4 complexed with K^+, and (d) TTE complexed with K^+. (e) Average bond lengths between the cations and the O atoms in the complexes. (f) Binding energies of different cations and solvent molecules.

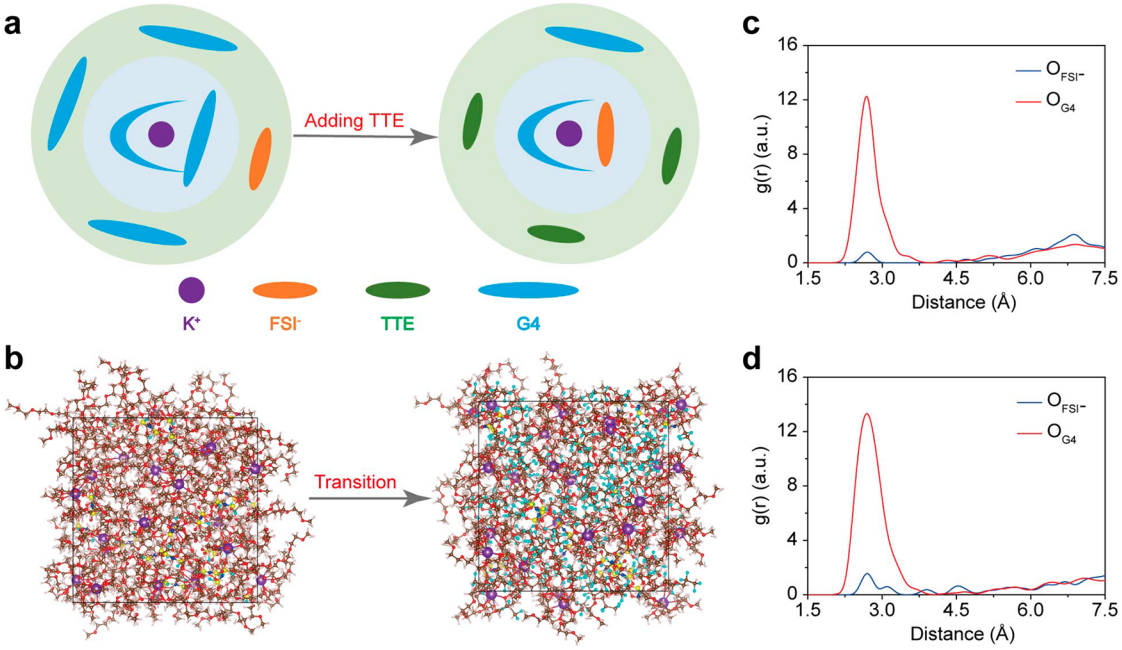

Figure 2. MD simulations of different solvation structures. (a) Schematic illustration of K^+ solvation structures in pure G4 (left) and in a mixture of G4 and TTE (right). (b) Snapshots of the optimized structures of KFSI in pure G4 (left) and KFSI in a mixture of G4 and TTE (right). H, F, O, N, C, S, and K atoms are represented by the colors pink, cyan, red, blue, brown, yellow, and purple, respectively. (c–d) Radial distribution functions of O_{G4} and O_{FSI}—atoms that are away from a fixed K ion: (c) in pure G4 and (d) in a mixture of G4 and TTE.

Herein, we study the solvation structures of potassium cations in a novel ether-based electrolyte, which was prepared from tetraethylene glycol dimethyl ether (G4), 1,1,2,2-tetrafluoroethyl-2,2,3,3-tetrafluoropropyl ether (TTE), and potassium bis(fluorosulfonyl)imide (KFSI) and investigate how the solvents solvate K^+ while enhancing the cycling stability of K metal anodes. Density functional theory (DFT) indicated that the G4 molecule provides multiple coordinating sites to chelate K^+ and molecular dynamics (MD) showed that the TTE additive facilitates the solvation effect. The intermolecular interactions of K^+ with the different components of the mixture solvent were examined using Raman and ^{17}O NMR spectroscopy. Compared to K//K symmetric cells that were prepared from a traditional electrolyte, cells that were prepared from the multidentate ether-based electrolyte that exhibited enhanced cycling stability (e.g., over 2000 h at

https://doi.org/10.1021/acsaem.2c01504
ACS Appl. Energy Mater. 2022, 5, 10366–10374

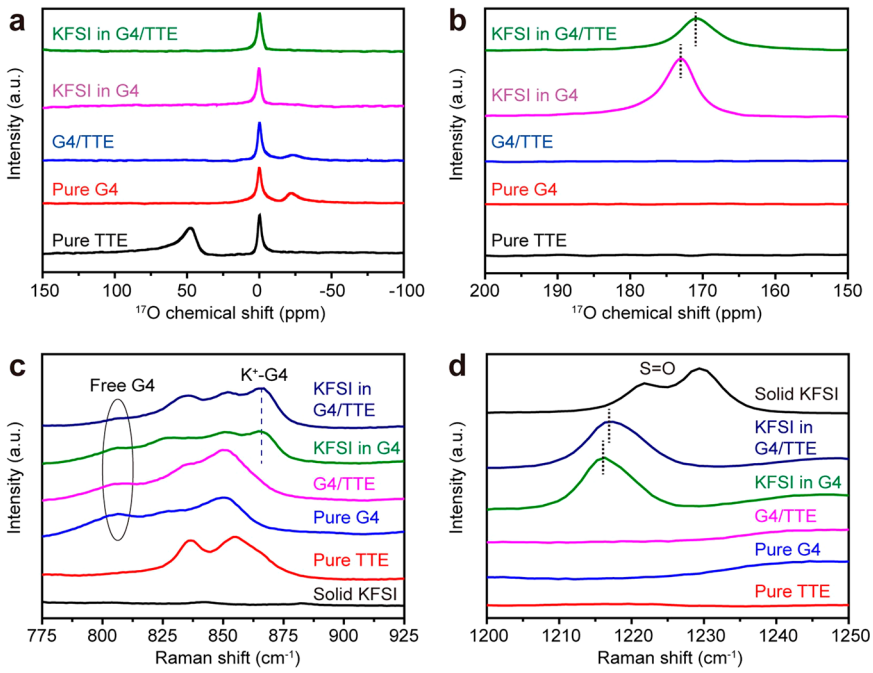

Figure 3. ^{17}O NMR and Raman spectra. (a, b) ^{17}O NMR spectra recorded for G4, TTE, G4/TTE (1.5:1 (v/v)), a solution of KFSI in G4 (1 M), and a solution of KFSI in G4/TTE (1 M): (a) over the range of 150 to −100 ppm and (b) over the range of 200 to 150 ppm. (c, d) Raman spectra recorded for different solvents, solid KFSI, and solutions of KFSI in the different solvents: (c) over the range of 775 to 925 cm^{-1} and (d) over the range of 1200 to 1250 cm^{-1}.

0.25 mA cm^{-2} under 0.25 mA h cm^{-2}), a result that was attributed to a suppression of K dendrite formation. In a broader context, the results and methodology described provide a new framework for designing high-performance electrolytes for K ion and K metal batteries.

The coordination structures formed between different solvents and cations including Li^+ or K^+ were first probed by density functional theory (DFT). Panels a and b of Figure 1 show that the coordination structures of a DME molecule and either Li^+ or K^+ feature ion−dipole interactions between the oxygen lone pairs of electrons and the metal cations. However, because K^+ is relatively large (radius = 1.38 Å) when compared with Li^+ (0.76 Å), the length of the K^+-O_{DME} bond is longer than that of the Li^+-O_{DME} bond (Figure 1e). As a result, the binding energy calculated for the former is significantly smaller than that calculated for the latter (Figure 1f). To enhance the solvation power of a K^+, G4, which contains five oxygen atoms, was selected because it can be expected to coordinate to K^+ in a multidentate fashion. Indeed, DFT indicated that K^+ can complex to all five oxygen atoms in G4 and afford a stable coordination structure (Figure 1c). Although the length of the K^+-O_{G4} bond (2.76 Å) is similar in length to that of the K^+-O_{DME} bond (2.67 Å) (Figure 1e), the binding energy between K^+ and G4 (−3.12 eV) is stronger than that calculated for Li^+ and DME (−3.04 eV) (Figure 1f). TTE was used as a cosolvent for the following reasons: (1) it facilitates the formation of KF in the solid−electrolyte interface (SEI) layer, (2) it reduces the viscosity of the electrolyte, and (3) it effectively adjusts the solvation structure of K ions with respect to the G4 additive. DFT was also used to assess TTE (Figure 1d). Due to the electron-withdrawing fluoro groups, the interaction between TTE and K^+ was found to be extremely weak (Figure 1f) and thus was not expected to compromise the intrinsic solvation power of G4.

The electrochemical performance of batteries is also affected by how the ions of the electrolyte salts are solvated. For example, the Li^+ and $TFSI^-$ ions of the LiTFSI salt exist as solvent-separated ion pairs (SSIPs) under dilute conditions (e.g., 1 M) in ether-based solvents, such as dioxolane (DOL) and/or DME, whereas the cations and anions exist as contact ion pairs (CIPs) or cation−anion aggregates (AGGs) upon concentration (e.g., 5 M).[17] Higher concentrations are reported to restrict the number of free solvent molecules, which, in turn, suppresses parasitic reactions between the lithium metal and solvent and thus improves the stability of the metal anode. It was hypothesized that a potassium metal anode may experience a similar effect in the presence the G4/TTE/KFSI electrolyte. According to the DFT calculations, G4 strongly solvates K^+ due to its multiple binding sites. As shown in Figure 2a (left panel), K^+ and FSI^- exist as SSIPs and thus are present in the first (light blue area) and second solvation shells (light green area), respectively. Adding TTE (right panel) may expel the FSI^- from the second solvation shell to the first solvation shell and thus cause the K^+ and FSI^- to form CIPs that are similar to those formed in highly concentrated electrolytes.

To test the hypothesis, the solvation structures of KFSI in pure G4 and in a mixture of G4 and TTE (1.5:1 (v/v)) were investigated by molecular dynamics (MD) simulations. The concentration of KFSI in both electrolytes was set to 1 M. Figure 2b shows snapshots of optimized structures of KFSI in pure G4 (left panel) and in a mixture of G4 and TTE (right panel). Due to the presence of excess G4, the KFSI is fully dissociated and K^+ and FSI^- exist in the form of SSIPs. This result implies that many free G4 molecules are still present and thus can potentially solvate additional cations or anions. In contrast, K^+ and FSI^- readily form CIPs upon the addition of TTE because the additive reduces the solvation power of the overall solvent and thus effectively decreases the number of

https://doi.org/10.1021/acsaem.2c01504
ACS Appl. Energy Mater. 2022, 5, 10366−10374

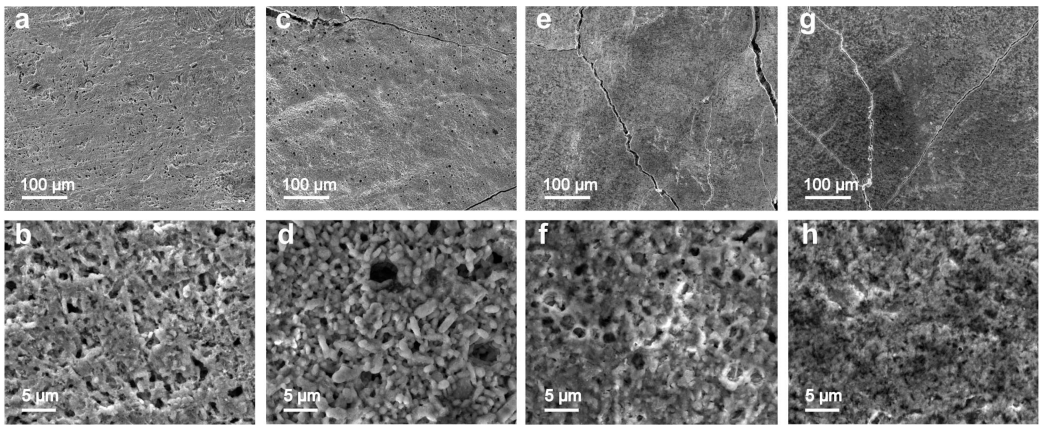

Figure 4. SEM characterization of K metal anodes before and after cycling: (a, b) pristine K foil, (c, d) after cycling in a solution of KFSI in DME (1 M), (e, f) after cycling in a solution of KFSI in G4 (1 M), and (g, h) after cycling in a solution of KFSI (1 M) in a mixture of G4 and TTE (1.5:1 (v/v)).

free G4 molecules. The solvation structures were further assessed by analyzing the oxygen atoms in G4 (denoted as O_{G4}) and the oxygen atoms in FSI^- (denoted as $O_{FSI}{}^-$) with the radial distribution function $g(r)$, which considers oxygen atoms in the shells that are away from a fixed K ion. In the case of pure G4 (Figure 2c), the $g(r)$ recorded for O_{G4} shows a major peak at ca. 2.7 Å and minor peak at ca. 6.9 Å, indicating that the first solvation shell is dominated by G4 molecules. In the $g(r)$ recorded for $O_{FSI}{}^-$, a major peak was found at ca. 6.9 Å, consistent with the FSI^- ions existing in the second solvation shell. As TTE is added to the electrolyte (Figure 2d), the first solvation shell remains unchanged and the characteristic peak of the second solvation shell disappears. Moreover, the major peak of the $g(r)$ function determined for the FSI^- is found at the position of the first solvation shell, which indicates that FSI^- ions entered the first solvation shell and formed CIPs with K ions. In other words, adding TTE to G4 regulates the cation and anion solvation structures by balancing the overall solvation power of the mixture.

The underlying intermolecular interactions formed between K^+ and the different solvents were further characterized using oxygen-17 nuclear magnetic resonance (^{17}O NMR) and Raman spectroscopy. The formation of Lewis acid−base type interactions between the G4 molecules and the K^+ ions leads to electron transfer from the former to the latter and thus alters the shielding effect of the electrons on the ether oxygen atoms.[18] As such, ^{17}O NMR spectroscopy is an effective tool for analyzing such intermolecular interactions. Figure 3a shows ^{17}O NMR spectra in a range that contains the characteristic signals of the various solvents. The chemical shift observed at −22 ppm in the spectrum of G4 was attributed to the terminal oxygen atoms (i.e., -(CH_2−O−CH_3)) of the molecule. The internal oxygen atom (i.e., -(CH_2−CH_2−O−CH_2−CH_2)-) was expected to give a signal at ca. −3 ppm,[19] but only a shoulder was observed due to the strong signal observed at 0 ppm, which stems from the reference solvent (D_2O). While TTE exhibited a broad signal at ca. 50 ppm, which was attributed to the ether oxygen atom (C−O−C) in the fluorinated molecule, only a signal characteristic of G4 was detected from a mixture of G4 and TTE (1.5:1 (v/v)) because the oxygen atoms in TTE accounted for a small proportion of the total oxygen content. Addition of KFSI to pure G4 or to the G4/TTE mixture led to the disappearance of the characteristic signals of G4, consistent with the solvation of the K^+ ions by G4 due to the formation of Lewis acid−base interactions. Since ^{17}O is a quadrupolar nucleus (nuclear spin: I = 5/2), the complexation of G4 and K^+ can lead to substantial signal broadening or even signal disappearance due to an increase in viscosity.[19] To verify the solvation structure of K^+, ^{17}O NMR spectra containing the signal of the FSI^- were further examined (Figure 3b). A signal at 172.7 ppm was detected upon analysis of a solution of KFSI in G4 and ascribed to the oxygen atoms of the sulfonyl group. When TTE was added, the signal shifted upfield and appeared at 170.6 ppm, a spectral change that may reflect the transformation of K^+ and FSI^- ions from SSIPs to CIPs.[19] The spectral change was consistent with the simulation data and confirmed that the TTE molecules caused the FSI^- ions to move from the second solvation shell to the first solvation shell and resulted in enhanced ion−dipole interactions. Note that KFSI is not soluble in TTE which prevented analysis of such a mixture.

Raman spectroscopy was also used to elucidate the solvation structures of K^+ in pure G4 and in the G4/TTE mixture. As shown in Figure 3c, the spectrum recorded for TTE exhibited Raman signals at 836 and 855 cm^{-1}. In comparison, signals between 800 and 860 cm^{-1} were observed in the spectrum recorded for G4 and assigned to a mixture of C−O−C stretching and CH_2 rocking vibration modes.[20] In the spectrum recorded for the G4/TTE mixture, the TTE signals at 836 and 855 cm^{-1} overlap with the G4 absorption bands at 827 and 850 cm^{-1}. Adding KFSI to G4 generates a new signal at 866 cm^{-1} due to the solvation of K^+ by G4 and leads to the formation of the K^+−G4 complex. As TTE was introduced into the solution of KFSI in G4, the characteristic signal assigned to the K^+−G4 complex became slightly stronger, whereas the signal that corresponds to free G4 (803 cm^{-1}) became weaker. Such spectroscopic changes could be ascribed to a decrease in the amount of the free G4 due to the addition of TTE. In other words, the solvation of K^+ by G4 increases as the FSI^- is expelled from the second solvation shell to the first solvation shell. Figure 3d shows additional Raman data that were collected to assess KFSI under various conditions. In blank tests, the pure solvents and their mixture show no spectral features in the pertinent region. Solid KFSI exhibits two signals at 1221 and 1230 cm^{-1} that can be ascribed to the sulfonyl group,[21] whereas a solution of KFSI in G4 exhibits one signal at 1216 cm^{-1} as the solvation of K^+ by G4 effectively separates the cation and the anion. Addition of TTE to the solution of

https://doi.org/10.1021/acsaem.2c01504
ACS Appl. Energy Mater. 2022, 5, 10366−10374

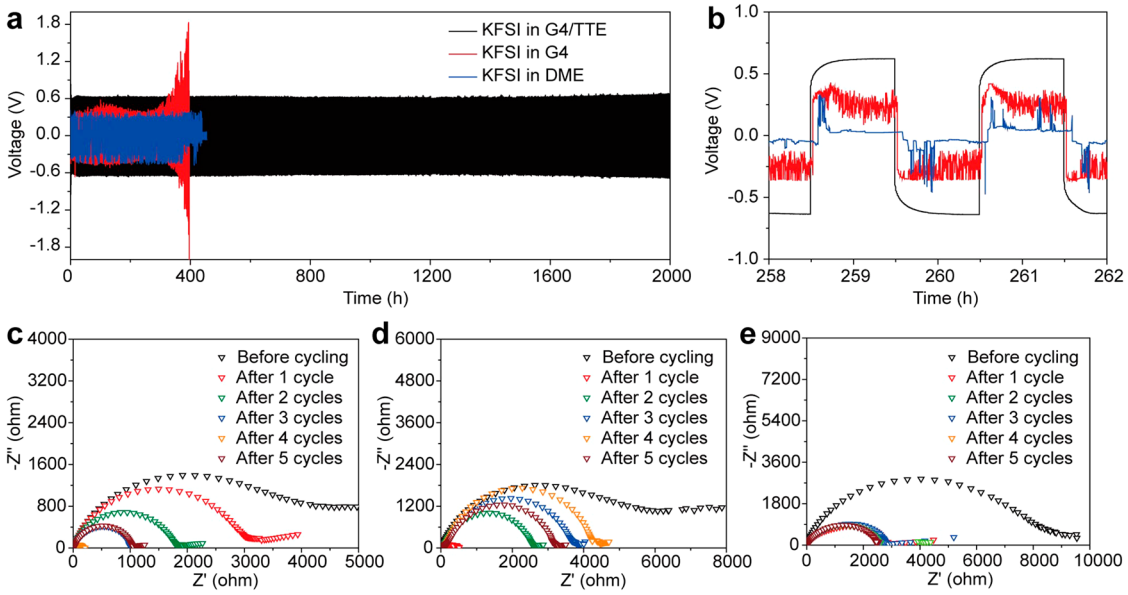

Figure 5. Symmetric cell characterization. (a) Polarization profiles recorded for K//K symmetric cells that were prepared from different electrolytes (indicated). (b) Enlarged view of two cycles of the polarization profiles from 258 to 262 h. (c–e) Nyquist plots recorded after multiple stripping–plating cycles (indicated) for the K//K symmetric cells prepared from (c) the DME-based electrolyte, (d) the G4-based electrolyte, and (e) the G4/TTE-based electrolyte.

KFSI in G4 resulted in a shift of the characteristic signal from 1216 to 1217 cm^{-1} (i.e., toward signals that are characteristic of solid KFSI). Such a spectroscopic shift is in accord with an increased interaction between the K^+ and FSI^- ions and consistent with the simulation data which indicated that TTE facilitates the formation of CIPs of K^+ and FSI^- (Figure 2). Collectively, the ^{17}O NMR and Raman data support the proposed solvation structure of K^+ formed with G4 and confirm that the addition of TTE can further regulate the solvation structure of K ions.

K//K symmetric cells were prepared to investigate the compatibilities of the different electrolytes with K metal electrodes. After five stripping–plating cycles that were conducted at 0.25 mA cm^{-2} under a capacity of 0.25 mA h cm^{-2}, the morphology changes of the K electrode were investigated using scanning electron microscopy (SEM). The pristine K foil showed a smooth surface with pores of approximately 1 μm in diameter. After cycling in the different electrolytes, the K foil exhibited smooth surfaces when observed at a relatively low magnification (Figures 4c,e,g). However, consistent with previous reports,[22] the K foil showed a mossy-like morphology with pits of approximately 5 μm in diameter after the stripping–plating cycles in the DME-based electrolyte under higher magnification (Figure 4d). In contrast, the K metal surface showed no mossy-like structures when cycled in a G4-based electrolyte (Figure 4f). Furthermore, the addition of TTE led to an improved morphology of the K foil electrode after cycling as a compact surface with no mossy-like structures was observed (Figure 4h). Likewise, dendrites or mossy-like structures were not observed at the K metal surfaces when higher current densities (i.e., 0.5 and 1 mA cm^{-2} under a capacity of 0.25 mA h cm^{-2}, Supporting Information Figure S1) were used. In addition, K//Cu cells were also prepared and tested in different electrolytes (Figure S2). The K deposited on the Cu foil in the G4/TTE-based electrolyte was found to be superior when compared with those obtained in the other two electrolytes. The different morphologies of the K electrode after the stripping–plating cycles in different electrolytes reflected the different compatibilities of the solvents with the K metal. Theoretical calculations indicated that the relative LUMO energies of the different solvents change in the following order: TTE < G4 < DME (Table S1). Thus, TTE is more prone to react with K metal and leads to the formation of KF in the solid–electrolyte interphase (SEI) layer during discharge (Figure S3).[23,24] According to previous reports,[13,25] KF should improve the conductivity of K^+ as well as consolidate current distribution. Therefore, the suppressed formation of K dendrites in G4/TTE-based electrolyte could be ascribed to the regulation of K metal deposition due to formation of the KF-containing SEI layer. By contrast, mossy-like structures were observed on the surface of K metal electrode in the DME- or G4-based electrolytes. In addition, the LSV tests performed in a three-electrode system exhibited no potential fluctuation until ca. 4.7 V (Figure S3) and thus the KFSI-G4/TTE (1.5:1 (v/v)) electrolyte appears to tolerate high potential windows (up to 4.5 V).

The surface properties of the K metal electrodes in the different electrolytes were further investigated using a polarization analysis and electrochemical impedance spectroscopy (EIS) of the K//K symmetric cells. Polarization profiles of the K//K cells were collected at 0.25 mA cm^{-2} under a capacity of 0.25 mA h cm^{-2} (Figure 5a). Although the polarization voltage recorded for the cell prepared from the G4/TTE-based electrolyte was relatively large, it remained stable when compared with those recorded from the cells that were prepared from the DME- or G4-based electrolytes. Close inspection revealed that the polarization profiles recorded for the cell prepared from the G4/TTE-based electrolyte was smooth with no overpotential (Figure 5b). By contrast, large overpotentials and significant fluctuations were observed in the polarization profiles recorded for the cells prepared using the other electrolytes. The smooth polarization profile with no overpotential could be ascribed to a stable SEI layer that formed on the surface of the K foil electrode in the G4/TTE-

https://doi.org/10.1021/acsaem.2c01504
ACS Appl. Energy Mater. 2022, 5, 10366–10374

based electrolyte, as opposed to the unstable SEI layers formed on the surface of the K foil in the other two electrolytes. The polarization voltage of the K//K cell prepared from DME-based electrolyte dropped after cycling for ~430 h on account of a short circuit inside the cell and the cell prepared from the G4-based electrolyte reached a large polarization voltage of ±5 V after cycling for ~390 h probably due to a gradual thickening of a SEI layer. In contrast, the cell prepared from the G4/TTE-based electrolyte remained stable, even after more than 2000 h of cycling. The excellent cycling stability was attributed to the dendrite-free surface of the K electrode as well as the formation of a resilient SEI layer that avoided uneven charge distribution and continuous consumption of electrolyte by the highly reactive K metal.

EIS data were collected for the different K//K symmetric cells after each of the first five stripping−plating cycles. The analyses were performed using a two-time-constant equivalent circuit (Figure S5 and Figure 5c−e). The bimodal feature of the −Phase−log(f) curves recorded for each cell reflect the equivalent circuit (Figure S6a−c). The feature at relatively high frequency was attributed to the interface between the current collector and the K foil, and the lower frequency one was assigned to the interface between the K foil and the electrolyte. Analyses of the key parameters associated with the interface of the K foil and the electrolyte indicated that the G4/TTE-based electrolyte facilitated the formation of stable SEI layer (Figure S6d,e). Initially, these cells exhibited relatively large charge-transfer resistance values (R_{ct} = ~4400, ~6000, and ~9000 Ω for the cells prepared from DME-, G4-, and G4/TTE-based electrolytes, respectively). However, after one stripping−plating cycle, R_{ct} dropped significantly (~3000, ~500, and ~2800 Ω for the cells prepared from DME-, G4-, and G4/TTE-based electrolytes, respectively). In the following stripping−plating cycles, the R_{ct} measured for the cell prepared from the G4/TTE-based electrolyte remained stable between 2500 and 2800 Ω (Figure 5e), a finding that reflects a stable SEI layer and is consistent with the data obtained from polarization test. In contrast, the R_{ct} measured for the cell prepared from the DME-based electrolyte fluctuated between 170 and 3000 Ω (Figure 5c), reflecting repeated formation of a new SEI layer due to the presence of K dendrites. The R_{ct} measured for the cell prepared from the G4-based electrolyte was found to increase from 500 to 4250 Ω as the cycling proceeded, consistent with a gradual thickening of the SEI layer. Consistent with literature reports,[26] the charge-transfer resistance (R_{ct}) values recorded for K//K cells were higher than those recorded for Li symmetric cells. The relatively large R_{ct} values recorded for the K//K cells can be ascribed to (1) deteriorated K electrode surfaces as they can readily react with trace water and oxygen during cell preparation and/or (2) delayed diffusion of K ions at the interface of the electrolyte and the K electrode due to the relatively large radius of K^+ (0.138 nm), particularly when compared with that of Li^+ (0.076 nm). These results were consistent with the SEM data and revealed how G4/TTE-based electrolytes can influence K deposition on the surfaces of K metal electrodes.

To further explore the use of the G4/TTE-based electrolyte in K metal batteries, potassium Prussian blue (KPB)//K half-cells were assembled and measured. As shown in Figure S7a, galvanostatic charge/discharge curves were recorded between 1.5 and 4.5 V as the electrolyte endures a relatively high potential window (up to 4.5 V). In the cycling test (Figure S7b), a specific capacity was initially measured to be 74.1 mA h g^{-1} at 40 mA g^{-1} and retained a value of 50.8 mA h g^{-1} after 300 cycles. The excellent cycling stability exhibited by the KPB//K cell prepared with the G4/TTE-based electrolyte was attributed to the stable stripping−plating process of the K metal on the anode.

In summary, the solvation structures of K^+ in a multidentate ether-based electrolyte that was comprised of G4, TTE, and KFSI were investigated by theoretical and experimental methods. Compared with commonly used ethers such as DME, G4 facilitates the formation of a relatively strong complex with K^+ via its multiple coordinating sites. The addition of TTE facilitates the K^+ and FSI^- ions to adopt a contact ion pair and promotes the ratio of G4 molecules that are involved in K^+ solvation. Theoretical and experimental data indicated that TTE is readily reduced and enables the formation of critical SEI layers and, as a result, K metal anodes in the ether-based electrolyte show a relatively constant R_{ct} values during stripping−plating cycles when compared with the values obtained from other electrolytes. For example, K//K symmetric cells prepared using the ether-based electrolyte can be subjected to stripping−plating cycling for over 2000 h, a result that is markedly improved when compared to cells that contain other electrolytes. In a broader perspective, the results described herein elucidate the solvation structures of K^+ in multidentate ether-based electrolytes and show how such details may be harnessed as a general approach for designing high-performance electrolytes for K-based batteries.

EXPERIMENTAL SECTION

Materials. Potassium metal (K, ≥99%) and 1,1,2,2-tetrafluoroethyl-2,2,3,3-tetrafluoropropyl ether (TTE, ≥98%) were purchased from Aladdin (Shanghai) Co., Ltd. Potassium bis(fluorosulfonyl) imide (KFSI, ≥98%) was obtained from J&K Scientific Co., Ltd. 1,2-Dimethoxyethane (DME, >99.99%) and tetraethylene glycol dimethyl ether (G4, >99.99%) were purchased from Shanghai Songjing New Energy Technology Co., Ltd. Potassium Prussian blue ($K_4Fe(CN)_6$, ≥99%) was obtained from Shanghai Macklin Biochemical Co., Ltd. Poly(vinylidene fluoride) (PVDF, ≥99.99%) was purchased from Sigma-Aldrich Co., Ltd. Ketjen black (KB, ≥99.99%) was obtained from Strem Chemicals, Inc. *N*-Methylpyrrolidone (NMP, ≥99%) was purchased from Xilong Chemical Co., Ltd. All chemicals were used as received.

Electrolyte Preparation. A solution of KFSI (1 M) in G4 and TTE (1.5:1 (v/v)) was prepared by dissolving KFSI (2.1976 mg, 10 mmol) in a mixture of G4 (6 mL) and TTE (4 mL). A solution of KFSI (1 M) in G4 was prepared by dissolving KFSI (2.1976 mg, 10 mmol) in G4 (10 mL). A solution of KFSI (1 M) in DME was prepared by dissolving KFSI (2.1976 mg, 10 mmol) in DME (10 mL). All operations were conducted in an argon-filled glovebox (H_2O < 0.1 ppm; O_2 > 0.1 ppm).

Cell Assembly and Electrochemical Measurement. A CR2032 coin type K//K symmetric cells were assembled for electrochemical measurements. K foils with thicknesses of ca. 1 mm were obtained by pressing pieces of K metal and cut into round disks with diameters of ca. 12 mm. CR2032 coin type cells were fabricated using the round K foil disks as electrodes and a piece of glass fiber membrane that was sandwiched by two pieces of polypropylene membranes as the separator. Electrolyte of 40 μL was separately added at the two sides of the separator. K//Cu half-cells were assembled using Cu foil as the cathode and K foil as the anode. Polypropylene and glass fiber membranes were placed on the cathode side and the anode side as separator. To prepare the KPB cathodes, KPB was first dried at 80 °C for 12 h and mixed with KB and PVDF at a mass ratio of 4:5:1 in NMP under stirring to form a slurry. The slurry was coated on Al current collector and dried at 80 °C for 12 h

https://doi.org/10.1021/acsaem.2c01504
ACS Appl. Energy Mater. 2022, 5, 10366−10374

in a vacuum oven. KPB//K cells were assembled using KPB as the cathode, K foil as the anode, Celgard2500 membrane as the separator, and a KFSI solution (1M) in G4/TTE (1.5:1 (v/v)) as the electrolyte. The area loading of KPB was ca. 1 mg cm^{-2}.

Galvanostatic charge/discharge curves of K//K symmetric cells, K//Cu half-cells, and KPB//K cells were collected on a CT2001A cell test instrument (LAND Electronic Co., Ltd.). Polarization tests of the K//K symmetric cells were performed under a capacity of 0.25 mA h cm^{-2} and at current densities of 0.25, 0.5, and 1 mA cm^{-2}. K//Cu half-cells in different electrolytes were measured at a current density of 0.25 mA cm^{-2} under a capacity of 0.25 mA h cm^{-2}. KPB//K cells were measured at 40 mA g^{-1} over a voltage range of 1.5−4.5 V. Linear sweep voltammetry (LSV) tests were performed from 0 to 7 V at a scan rate of 2 mV s^{-1} on a CHI 760E electrochemical workstation. LSV data were collected using a three-electrode system with a glassy carbon electrode as the working electrode, a piece of Pt foil as the counter electrode, and a piece of K foil as the reference electrode. Electrochemical impedance spectroscopy (EIS) measurements were performed on the same electrochemical workstation with amplitude of 10 mV over a frequency range of 100 kHz to 0.01 Hz.

Characterization. Raman spectra were recorded on a Renishaw inVia Reflex microscope spectrometer using an excitation wavelength of 785 nm at room temperature. The samples were sealed in capillaries with the inner diameter of 0.3 mm and fixed on the glass slides. The ^{17}O NMR spectra were acquired on a Bruker Avance III 400 MHz NMR spectrometer at a ^{17}O frequency of 54.24 MHz and D_2O was used as an external reference set to 0 ppm. The ^{17}O 90° pulse length was calibrated at 40 μs. A TRIP pulse sequence[27] was used to accumulate the signal of ^{17}O with a recycle delay of 0.4 s. SEM images were collected on a JEOL JSM-7800F scanning electron microscope operated at an acceleration voltage of 10 kV. The samples used for SEM observations were obtained by disassembling the K//K symmetric cells and K//Cu half-cells in an argon-filled glovebox. And the K foil electrodes were rinsed with DME in an argon-filled glovebox.

DFT Calculations and MD Simulations. The coordination structures and binding strengths of Li^+ and K^+ with different solvent molecules were calculated using the VASP code with the projector-augmented wave (PAW).[28] The Perdew−Burke−Ernzerhof (PBE) form of the exchange−correlations functional was employed in the simulation with the plane-wave cutoff of 450 eV,[29] and the long-range interlayer van der Waals (vdW) interaction was described with the DFT-D2 method.[30] A large cell with lattice parameters of 15 Å was used in the simulations, whose *k*-point mesh was 1 × 1 × 1. The structures were optimized by using the conjugate gradient method, in which the convergence for total energy and interaction force was set to be 10^{-6} eV and 10^{-3} eV $Å^{-1}$, respectively. Energy levels of HOMO and LUMO were obtained by analyzing the occupation of bands. The binding strengths were calculated following the equation $E = E_{total} - E_{ion} - E_{sol}$, where E_{total}, E_{ion}, and E_{sol} are the total energy of solvent with adsorbed ion, the energy of solvent, and the energy of ion. MD calculations were performed to determine the solvation structures of K^+ in pure G4 and a mixture of G4 and TTE using the Forcite module and the COMPASS force field as implemented in Materials studios. According to experimental data, a system consisting of 20 KFSI molecules randomly distributed in 90 G4 molecules was constructed to describe the solvation structure of K^+ in pure G4. As for the solvation structure of K^+ in G4 and TTE, a system was constructed by randomly distributing 20 KFSI molecules in to 54 G4 molecules and 54 TTE molecules. Each system was relaxed in the *NPT* ensemble at T = 298 K and pressure = 1 atm for 30 ns with a time step of 0.5 fs. Then, the radial distribution functions (RDF) were calculated based on the relaxed structure.

■ ASSOCIATED CONTENT

Supporting Information

The Supporting Information is available free of charge at https://pubs.acs.org/doi/10.1021/acsaem.2c01504.

SEM images; HOMO and LUMO energy levels; LSV profiles; equivalent circuit model used to fit the EIS data; additional analyses of the EIS data (PDF)

■ AUTHOR INFORMATION

Corresponding Author

Jianxin Geng − *State Key Laboratory of Separation Membranes and Membrane Processes; Tianjin Key Laboratory of Advanced Fibers and Energy Storage; School of Material Science and Engineering, Tiangong University, Tianjin 300387, China;* orcid.org/0000-0003-0428-4621; Email: jianxingeng@tiangong.edu.cn

Authors

Chao Chen − *State Key Laboratory of Organic−Inorganic Composites; Beijing Advanced Innovation Center for Soft Matter Science and Engineering, Beijing University of Chemical Technology, Beijing 100029, China*

Ji Zhou − *State Key Laboratory of Organic−Inorganic Composites; Beijing Advanced Innovation Center for Soft Matter Science and Engineering, Beijing University of Chemical Technology, Beijing 100029, China*

Wenbin Gong − *School of Physics and Energy, Xuzhou University of Technology, Xuzhou 221018, China;* orcid.org/0000-0002-6699-0954

Xueying Fan − *State Key Laboratory of Organic−Inorganic Composites; Beijing Advanced Innovation Center for Soft Matter Science and Engineering, Beijing University of Chemical Technology, Beijing 100029, China*

Xiaodong Meng − *State Key Laboratory of Organic−Inorganic Composites; Beijing Advanced Innovation Center for Soft Matter Science and Engineering, Beijing University of Chemical Technology, Beijing 100029, China*

Shang Chen − *State Key Laboratory of Organic−Inorganic Composites; Beijing Advanced Innovation Center for Soft Matter Science and Engineering, Beijing University of Chemical Technology, Beijing 100029, China*

Longhua Sun − *State Key Laboratory of Organic−Inorganic Composites; Beijing Advanced Innovation Center for Soft Matter Science and Engineering, Beijing University of Chemical Technology, Beijing 100029, China*

Yongqiang Meng − *State Key Laboratory of Organic−Inorganic Composites; Beijing Advanced Innovation Center for Soft Matter Science and Engineering, Beijing University of Chemical Technology, Beijing 100029, China*

Kangjia Tao − *State Key Laboratory of Organic−Inorganic Composites; Beijing Advanced Innovation Center for Soft Matter Science and Engineering, Beijing University of Chemical Technology, Beijing 100029, China*

Burak Ülgüt − *Faculty of Science, Department of Chemistry, Bilkent University, 06800 Ankara, Türkiye*

Pingchuan Sun − *Key Laboratory of Functional Polymer Materials of the Ministry of Education and College of Chemistry and State Key Laboratory of Medicinal Chemical Biology, Nankai University, Tianjin 300071, China;* orcid.org/0000-0002-5603-6462

Christopher W. Bielawski − *Center for Multidimensional Carbon Materials (CMCM), Institute for Basic Science (IBS), Ulsan 44919, Republic of Korea; Department of Chemistry, Ulsan National Institute of Science and Technology (UNIST), Ulsan 44919, Republic of Korea;* orcid.org/0000-0002-0520-1982

https://doi.org/10.1021/acsaem.2c01504
ACS Appl. Energy Mater. 2022, 5, 10366−10374

Complete contact information is available at:
https://pubs.acs.org/10.1021/acsaem.2c01504

Author Contributions

[○]C.C. and J.Z. contributed equally to this work.

Notes

The authors declare no competing financial interest.

■ ACKNOWLEDGMENTS

This work was supported by the National Natural Science Foundation of China (21961160700), the National High Level Talents Special Support Plan of China, and the IBS (IBS-R019-D1).

■ REFERENCES

(1) Cao, Y.; Jia, Y.; Meng, X.; Fan, X.; Zhang, J.; Zhou, J.; Matoga, D.; Bielawski, C. W.; Geng, J. Covalently Grafting Conjugated Porous Polymers to Mxene Offers a Two-Dimensional Sandwich-Structured Electrocatalytic Sulfur Host for Lithium-Sulfur Batteries. *Chem. Eng. J.* **2022**, *446*, 137365.

(2) Jia, Y.; Gong, W.; Fan, X.; Chen, S.; Meng, X.; Meng, Y.; Zhou, J.; Cao, Y.; Hong, S.; Zheng, L.; Wang, Z.; Bielawski, C. W.; Geng, J. Coaxially Grafting Conjugated Microporous Polymers Containing Single-Atom Cobalt Catalysts to Carbon Nanotubes Enhances Sulfur Cathode Reaction Kinetics. *Chem. Eng. J.* **2022**, *444*, 136546.

(3) Ma, J. P.; Fan, J. B.; Chen, S.; Yang, X. Y.; Hui, K. N.; Zhang, H. W.; Bielawski, C. W.; Geng, J. X. Covalent Confinement of Sulfur Copolymers onto Graphene Sheets Affords Ultrastable Lithium-Sulfur Batteries with Fast Cathode Kinetics. *ACS Appl. Mater. Interfaces* **2019**, *11* (14), 13234−13243.

(4) Meng, X.; Liu, X.; Fan, X.; Chen, X.; Chen, S.; Meng, Y.; Wang, M.; Zhou, J.; Hong, S.; Zheng, L.; Shi, G.; Bielawski, C. W.; Geng, J. Single-Atom Catalyst Aggregates: Size-Matching Is Critical to Electrocatalytic Performance in Sulfur Cathodes. *Adv. Sci.* **2022**, *9* (3), 2103773.

(5) Park, J.; Lee, J.; Alfaruqi, M. H.; Kwak, W.-J.; Kim, J.; Hwang, J.-Y. Initial Investigation and Evaluation of Potassium Metal as an Anode for Rechargeable Potassium Batteries. *J. Mater. Chem. A* **2020**, *8* (33), 16718−16737.

(6) Xue, L.; Gao, H.; Zhou, W.; Xin, S.; Park, K.; Li, Y.; Goodenough, J. B. Liquid K-Na Alloy Anode Enables Dendrite-Free Potassium Batteries. *Adv. Mater.* **2016**, *28* (43), 9608−9612.

(7) Wang, H.; Hu, J.; Dong, J.; Lau, K. C.; Qin, L.; Lei, Y.; Li, B.; Zhai, D.; Wu, Y.; Kang, F. Artificial Solid-Electrolyte Interphase Enabled High-Capacity and Stable Cycling Potassium Metal Batteries. *Adv. Energy Mater.* **2019**, *9* (43), 1902697.

(8) Tang, X.; Zhou, D.; Li, P.; Guo, X.; Sun, B.; Liu, H.; Yan, K.; Gogotsi, Y.; Wang, G. Mxene-Based Dendrite-Free Potassium Metal Batteries. *Adv. Mater.* **2020**, *32* (4), 1906739.

(9) Wang, S.; Yan, Y.; Xiong, D.; Li, G.; Wang, Y.; Chen, F.; Chen, S.; Tian, B.; Shi, Y. Towards Dendrite-Free Potassium-Metal Batteries: Rational Design of a Multifunctional 3D Polyvinyl Alcohol-Borax Layer. *Angew. Chem., Int. Ed.* **2021**, *60* (47), 25122−25127.

(10) Gu, Y.; Wang, W.-W.; Li, Y.-J.; Wu, Q.-H.; Tang, S.; Yan, J.-W.; Zheng, M.-S.; Wu, D.-Y.; Fan, C.-H.; Hu, W.-Q.; Chen, Z.-B.; Fang, Y.; Zhang, Q.-H.; Dong, Q.-F.; Mao, B.-W. Designable Ultra-Smooth Ultra-Thin Solid-Electrolyte Interphases of Three Alkali Metal Anodes. *Nat. Commun.* **2018**, *9*, 1339.

(11) Pham, T. A.; Kweon, K. E.; Samanta, A.; Lordi, V.; Pask, J. E. Solvation and Dynamics of Sodium and Potassium in Ethylene Carbonate from ab Initio Molecular Dynamics Simulations. *J. Phys. Chem. C* **2017**, *121* (40), 21913−21920.

(12) Xiao, N.; McCulloch, W. D.; Wu, Y. Reversible Dendrite-Free Potassium Plating and Stripping Electrochemistry for Potassium Secondary Batteries. *J. Am. Chem. Soc.* **2017**, *139* (28), 9475−9478.

(13) Wang, H.; Dong, J.; Guo, Q.; Xu, W.; Zhang, H.; Lau, K. C.; Wei, Y.; Hu, J.; Zhai, D.; Kang, F. Highly Stable Potassium Metal Batteries Enabled by Regulating Surface Chemistry in Ether Electrolyte. *Energy Storage Mater.* **2021**, *42*, 526−532.

(14) Touja, J.; Le Pham, P. N.; Louvain, N.; Monconduit, L.; Stievano, L. Effect of the Electrolyte on K-Metal Batteries. *Chem. Commun.* **2020**, *56* (93), 14673−14676.

(15) Sun, H.; Liang, P.; Zhu, G.; Hung, W. H.; Li, Y.-Y.; Tai, H.-C.; Huang, C.-L.; Li, J.; Meng, Y.; Angell, M.; Wang, C.-A.; Dai, H. A High-Performance Potassium Metal Battery Using Safe Ionic Liquid Electrolyte. *Proc. Natl. Acad. Sci. U.S.A.* **2020**, *117* (45), 27847−27853.

(16) Zhang, Y.; Bahi, A.; Ko, F.; Liu, J. Polyacrylonitrile-Reinforced Composite Gel Polymer Electrolytes for Stable Potassium Metal Anodes. *Small* **2022**, *18* (8), 2107186.

(17) Amine, R.; Liu, J. Z.; Acznik, I.; Sheng, T.; Lota, K.; Sun, H.; Sun, C. J.; Fic, K.; Zuo, X. B.; Ren, Y.; El-Hady, D. A.; Alshitari, W.; Al-Bogami, A. S.; Chen, Z. H.; Amine, K.; Xu, G. L. Regulating the Hidden Solvation-Ion-Exchange in Concentrated Electrolytes for Stable and Safe Lithium Metal Batteries. *Adv. Energy Mater.* **2020**, *10* (25), 2000901.

(18) Bogle, X.; Vazquez, R.; Greenbaum, S.; Cresce, A. v. W.; Xu, K. Understanding Li^+-Solvent Interaction in Nonaqueous Carbonate Electrolytes with ^{17}O NMR. *J. Phys. Chem. Lett.* **2013**, *4* (10), 1664−1668.

(19) Ruggeri, I.; La Monaca, A.; De Giorgio, F.; Soavi, F.; Arbizzani, C.; Berbenni, V.; Ferrara, C.; Mustarelli, P. Correlating Structure and Properties of Super-Concentrated Electrolyte Solutions: ^{17}O NMR and Electrochemical Characterization. *ChemElectroChem.* **2019**, *6* (15), 4002−4009.

(20) Ueno, K.; Tatara, R.; Tsuzuki, S.; Saito, S.; Doi, H.; Yoshida, K.; Mandai, T.; Matsugami, M.; Umebayashi, Y.; Dokko, K.; Watanabe, M. Li^+ Solvation in Glyme-Li Salt Solvate Ionic Liquids. *Phys. Chem. Chem. Phys.* **2015**, *17* (12), 8248−8257.

(21) Yang, H.; Guo, C.; Chen, J.; Naveed, A.; Yang, J.; Nuli, Y.; Wang, J. An Intrinsic Flame-Retardant Organic Electrolyte for Safe Lithium-Sulfur Batteries. *Angew. Chem., Int. Ed.* **2019**, *58* (3), 791−795.

(22) Ding, J.-F.; Xu, R.; Yao, N.; Chen, X.; Xiao, Y.; Yao, Y.-X.; Yan, C.; Xie, J.; Huang, J.-Q. Non-Solvating and Low-Dielectricity Cosolvent for Anion-Derived Solid Electrolyte Interphases in Lithium Metal Batteries. *Angew. Chem., Int. Ed.* **2021**, *60* (20), 11442−11447.

(23) Zhao, H.; Gu, J.; Gao, Y.; Hou, Q.; Ren, Z.; Qi, Y.; Zhang, K.; Shen, C.; Zhang, J.; Xie, K. A Multifunctional Electrolyte with Highly-Coordinated Solvation Structure-in-Nonsolvent for Rechargeable Lithium Batteries. *J. Energy Chem.* **2020**, *51*, 362−371.

(24) Zhao, Q.; Zhang, Y.; Sun, G.; Cong, L.; Sun, L.; Xie, H.; Liu, J. Binary Mixtures of Highly Concentrated Tetraglyme and Hydrofluoroether as a Stable and Nonflammable Electrolyte for Li-O_2 Batteries. *ACS Appl. Mater. Interfaces* **2018**, *10* (31), 26312−26319.

(25) Liu, S.; Mao, J.; Zhang, Q.; Wang, Z.; Pang, W. K.; Zhang, L.; Du, A.; Sencadas, V.; Zhang, W.; Guo, Z. An Intrinsically Non-Flammable Electrolyte for High-Performance Potassium Batteries. *Angew. Chem., Int. Ed.* **2020**, *59* (9), 3638−3644.

(26) Iermakova, D. I.; Dugas, R.; Palacin, M. R.; Ponrouch, A. On the Comparative Stability of Li and Na Metal Anode Interfaces in Conventional Alkyl Carbonate Electrolytes. *J. Electrochem. Soc.* **2015**, *162* (13), A7060−A7066.

(27) Wang, F.; Ramakrishna, S. K.; Sun, P.; Fu, R. Triple-Pulse Excitation: An Efficient Way for Suppressing Background Signals and Eliminating Radio-Frequency Acoustic Ringing in Direct Polarization Nmr Experiments. *J. Magn. Reson.* **2021**, *332*, 107067.

(28) Blöchl, P. E. Projector Augmented-Wave Method. *Phys. Rev., B* **1994**, *50* (24), 17953−17979.

(29) Perdew, J. P.; Burke, K.; Ernzerhof, M. Generalized Gradient Approximation Made Simple. *Phys. Rev. Lett.* **1996**, *77* (18), 3865−3868.

(30) Grimme, S. Semiempirical Gga-Type Density Functional Constructed with a Long-Range Dispersion Correction. *J. Comput. Chem.* **2006**, *27* (15), 1787−1799.

https://doi.org/10.1021/acsaem.2c01504
ACS Appl. Energy Mater. 2022, 5, 10366−10374